Research Square

Preprints are preliminary reports that have not undergone peer review.
They should not be considered conclusive, used to inform clinical practice,
or referenced by the media as validated information.

Cellular reconfiguration of Alzheimer's disease genetic susceptibility across aging and pathology

Ziang Meng
Center for Bioinformatics, Faculty of Computing, Harbin Institute of Technology, Harbin 150001, China.
Yingchao Song
College of Medical Information and Artificial Intelligence, Shandong First Medical University, Shandong, China.
Xianjin Wang
College of Medical Information and Artificial Intelligence, Shandong First Medical University, Shandong, China.
Maowen Ba
Department of Neurology, Yantai Yuhuangding Hospital, Qingdao University, Yantai, Shandong, China.
Siru Wang
College of Medical Information and Artificial Intelligence, Shandong First Medical University, Shandong, China.
Ziming Cui
Department of Computer and Data Sciences, Case Western Reserve University, Cleveland, OH 44106, USA.
Xiaoli Ma
Central Hospital Affiliated to Shandong First Medical University
Tao Xin
Shandong First Medical University & Shandong Academy of Medical Sciences
Xiao Chang
changx@email.chop.edu

Shandong First Medical University
Tao Jiang
Harbin Institute of Technology

Article

Keywords:

Posted Date: November 19th, 2026

DOI: https://doi.org/10.21203/rs.3.rs-11690101/v1

License: This work is licensed under a Creative Commons Attribution 4.0 International License.
Read Full License

Additional Declarations: No competing interests reported.

Cellular reconfiguration of Alzheimer's disease genetic susceptibility across aging and pathology

Ziang Meng[1], Yingchao Song[2], Xianjin Wang[2], Maowen Ba[3,4], Siru Wang[2], Ziming Cui[5], Xiaoli Ma[6], Tao Xin[7,†], Xiao Chang[2,3,†], Tao Jiang[1,8,†]

[1] Center for Bioinformatics, Faculty of Computing, Harbin Institute of Technology, Harbin 150001, China.

[2] College of Medical Information and Artificial Intelligence, Shandong First Medical University, Shandong, China.

[3] Department of Neurology, Yantai Yuhuangding Hospital, Qingdao University, Yantai, Shandong, China.

[4] Shandong Provincial Key Laboratory of Neuroimmune Interaction and Regulation, Yantai, Shandong, China.

[5] Department of Computer and Data Sciences, Case Western Reserve University, Cleveland, OH 44106, USA.

[6] Center for Basic and Translational Medical Research, Central Hospital Affiliated to Shandong First Medical University, Jinan, Shandong, China.

[7] Department of Neurosurgery, The First Affiliated Hospital of Shandong First Medical University & Shandong Provincial Qianfoshan Hospital, Jinan 250014, China.

[8] Zhengzhou Research Institute, Harbin Institute of Technology, Zhengzhou, Henan 450000, China.

† Corresponding authors:

Tao Jiang: tjiang@hit.edu.cn

Tao Xin: drxintao@yeah.net

Xiao Chang: changx@email.chop.edu

Abstract

Genome-wide association studies identify Alzheimer's disease (AD) susceptibility genes, but understanding how these genetic signals are organized across ageing, disease progression and cell types is a fundamental biological challenge. We developed single-cell Genetically Informed Perturbation Analysis (scGIPA) to integrate AD associations, brain regulatory evidence and hippocampal single-nucleus transcriptomes, resolving cellular contributions and genetic-route dependence through in silico perturbation. Across healthy ageing and early and later pathology, six overlapping functional modules showed stage-dependent cellular configurations; lipid-clearance and amyloid-fibril-regulation contributions peaked in early pathology. Of 1,469 AD-associated genes, 349 contributed to both ageing and pathology, representing 50.2% of participating genes. Genes contributing to both ageing and pathology preferentially retained contributions in the same cell types and were enriched in an external microglial co-expression module. *PVR* and *HBEGF* highlighted endothelial ageing, whereas *APOE* and *BIN1* showed changing cellular contributions and genetic-route dependence across stages. Our findings reveal how AD susceptibility is reorganized across ageing and pathology within interconnected vascular, glial and neuronal programmes.

Main

Alzheimer disease (AD) develops in an ageing brain through progressive changes involving vascular, immune and neuronal cells. The recent consensus genome-wide association meta-analysis expanded the genetic landscape of AD to 91 loci associated with AD and related dementias.[1] These genetic associations implicate diverse biological processes, including lipid handling, endosomal transport, immune regulation and amyloid-related functions. However, identifying genetic susceptibility loci provides only a partial view of how the implicated genes contribute to ageing and disease progression, particularly as their cellular actions remain incompletely resolved. Emerging frameworks suggest that AD progression involves transitions between cellular states shaped by declining homeostatic resilience and biological thresholds.[2] Spatial and single-nucleus studies further reveal heterogeneous microglial and neuronal responses across the amyloid-β–tau transition, pathological stages and brain regions.[3,4,5,6] A central biological question is therefore how genes implicated by AD GWAS are functionally organized across the transition from healthy ageing to early and later pathology, and whether genes contributing across stages retain similar cellular roles or undergo changes in their functional contributions.

Recent computational advances and cell-type eQTL maps have begun to bridge genetic susceptibility and cellular biology.[7] Integrative approaches such as scDRS identify individual cells enriched for the expression of GWAS-implicated genes, whereas scPRS combines graph neural networks with single-cell chromatin accessibility to resolve the cellular and regulatory organization of polygenic risk.[8,9] In parallel, artificial intelligence has transformed the analysis of single-cell transcriptomes. Deep generative models such as scVI learn probabilistic representations of cellular expression states, while scGen predicts transcriptional responses to perturbations.[10,11] More recent frameworks, including GEARS and scGPT, extend these capabilities towards predicting genetic perturbation responses and learning transferable representations of cellular biology.[12,13] These developments offer new opportunities to move beyond identifying disease-associated genes and cell types towards understanding how genetic susceptibility is expressed across changing cellular states. However, comparing the contributions of individual GWAS-implicated genes across healthy ageing and successive pathological states requires approaches that distinguish changes in cellular expression from those associated with genetic regulatory inputs. Integrating genetic regulatory evidence into cellular-state models enables in silico perturbations to examine how gene contributions change when expression or genetic inputs are altered within a common cellular context. Such analyses may help resolve the stage-dependent functional organization of AD susceptibility genes and their connections across vascular, glial and neuronal programmes.

Here, we developed an integrative computational framework to investigate how AD genetic susceptibility is organized across ageing and disease progression. Using a human hippocampal single-nucleus atlas spanning young adulthood, healthy ageing, intermediate pathology and AD,[14] we combined cellular transcriptomes with AD GWAS associations and brain regulatory evidence to characterize the contributions of genetically implicated genes across successive stages. Through complementary in silico perturbations of gene expression and genetic regulatory inputs, we assessed expression-state contributions and genetic-route dependence within a common cellular context. We then examined how these contributions were distributed across functional modules, distinguished genes involved in ageing, pathology or both, and investigated whether genes contributing to both retained their contributions in the same cell types across stages. This framework enabled us to investigate how AD-associated genetic susceptibility connects ageing and pathology through both retained contributions in the same cell types and stage-dependent functional contributions.

Results

Development of scGIPA for genetically informed counterfactual modelling

To locate genes implicated by AD GWAS within the ageing–pathology sequence, we developed scGIPA (single-cell Genetically Informed Perturbation Analysis), an integrative computational framework that examines their expression-state contributions and genetic-route dependence across cellular contexts. The framework uses two complementary in silico perturbations—expression restoration and genetic-input masking—to assess how individual genes contribute to the distinction between successive stages of ageing and pathology (Fig. 1).

We defined two counterfactual readouts to distinguish these complementary dimensions of gene contribution (Fig. 1d). Expression-state contribution (*I*) measures how restoring a gene's observed expression to its earlier-stage reference alters the model's recognition of the later state, including changes propagated through expression-weighted regulatory inputs. Genetic-route dependence (*M*) measures the corresponding effect of masking the GWAS/eQTL-informed regulatory input associated with that gene and cell type, while preserving its observed expression profile and expression-derived representation. Both readouts are calculated as the original stage margin minus the perturbed stage margin. The stage margin is defined as the later-state classifier logit minus the earlier-state logit. Positive values indicate that the perturbation reduces recognition of the later state relative to the earlier state, whereas negative values indicate the opposite. Thus, *I* captures the contribution of a gene's expression configuration to stage discrimination, whereas *M* evaluates the additional contribution of its genetically informed regulatory route at the same expression state. Their signs reflect model responses to perturbation rather than the direction of gene expression changes or assignment to a particular disease stage.

We applied this framework to three adjacent transitions: young adulthood to healthy ageing (YA to HA), healthy ageing to preclinical intermediate pathology (HA to PCI), and intermediate pathology to AD (PCI to AD). The hippocampal single-nucleus dataset comprised 131,869 nuclei across 13 annotated cell types from 33 donors, including eight YA, nine HA, six PCI and ten AD donors (Supplementary Table 1). AD GWAS signals were linked to genes using SingleBrain cell-type-specific cis-eQTLs derived from single-cell data, with BrainMeta cortical cis-eQTLs supplementing cell types without SingleBrain coverage[15,16]. Together with MAGMA gene-level evidence, this defined 3,087 gene–cell regulatory routes, which were combined with gene expression and cell identity to model cellular states through classification and expression reconstruction (Fig. 1a–c and Supplementary Tables 2–7).

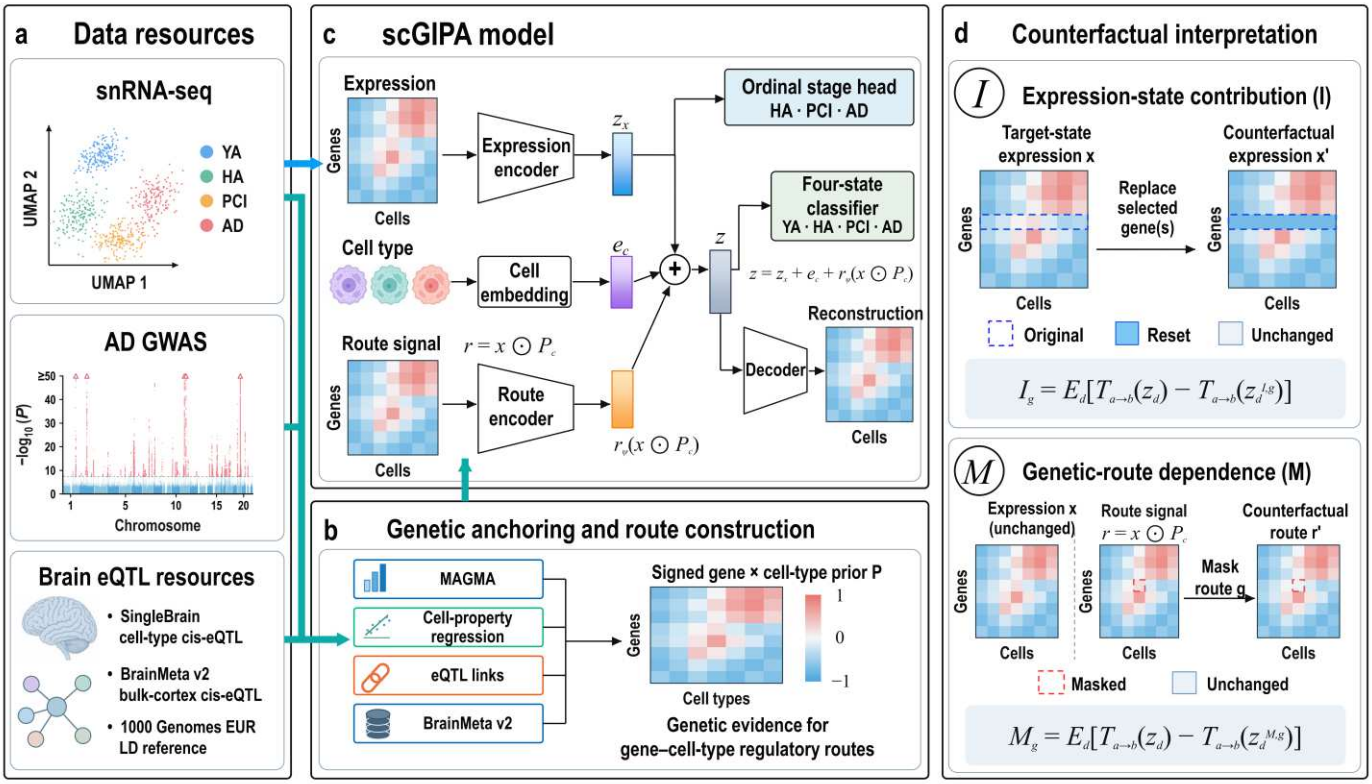


Fig. 1 | Overview of scGIPA and its counterfactual interpretation. a, Hippocampal single-nucleus RNA sequencing, AD GWAS and brain eQTL resources. The Manhattan plot shows the study GWAS; coral marks $P < 5 \times 10^{-8}$. Open triangles mark signals beyond the plotted range. b, Integration of MAGMA associations, cell-type enrichment and eQTL evidence into 3,087 gene–cell regulatory routes. c, Expression, cell identity and genetic-route signals are combined for state classification and expression reconstruction, with an auxiliary ordinal-stage head. d, Expression-state contribution (I) is assessed by restoring selected expression values to the earlier-state reference; genetic-route dependence (M) is assessed by masking selected routes while holding expression fixed. Effects are original-minus-perturbed differences in the later-versus-earlier stage margin; positive values indicate a lower margin after perturbation and negative values a higher margin.

Model validation and prioritization of genetically informed gene–cell routes

We first evaluated whether scGIPA could distinguish successive stages of ageing and pathology using repeated donor-validation partitions (Fig. 2a). scGIPA achieved donor-level receiver operating characteristic area under the curve (ROC AUC) values of 0.917 for YA to HA, 0.833 for HA to PCI and 0.867 for PCI to AD, with significant discrimination in all three comparisons (one-sided exact donor-label permutation, P = 0.0012, 0.018 and 0.0080, respectively). Across these transitions, scGIPA showed higher AUCs than logistic regression, linear support vector machines and random forests, although the difference from random forests was smaller for PCI to AD. These results support the ability of the integrated model to distinguish cellular states across both healthy ageing and pathological progression.

We next examined whether scGIPA could prioritize gene–cell routes that retained information about pathological transitions (Fig. 2b). Candidate panels containing 10, 20 or 30 genes per cell type were selected using four validation splits and evaluated in the omitted split. For HA to PCI, scGIPA-prioritized panels achieved pooled-record AUCs of 0.88–0.97, compared with 0.35–0.46 for MAGMA-based panels and 0.61–0.69 for brain transcriptome-wide association study (TWAS) panels. For PCI to AD, scGIPA panels achieved AUCs of 0.82–0.86, compared with 0.55–0.71 for MAGMA and 0.59–0.69 for brain TWAS. These comparisons indicate that scGIPA prioritization retained stage-discriminative information that was not equivalently captured by gene-level association or TWAS-based selection alone.

Finally, we assessed whether prioritized genes exhibited reproducible counterfactual contributions beyond those expected from matched random panels (Fig. 2c,d). Across five validation splits, the mean absolute expression-state contribution (*I*) was enriched by 5.95-, 8.63- and 8.82-fold for YA to HA, HA to PCI and PCI to AD, respectively, relative to matched random panels (empirical P = 0.001 for each comparison). Genetic-route dependence (*M*) showed corresponding enrichments of 3.85-, 4.36- and 4.50-fold (empirical P = 0.001 for each comparison). The consistent enrichment of both readouts across successive transitions supports the reproducibility of scGIPA's counterfactual prioritization and provides a basis for investigating how genetically implicated genes contribute to cellular changes during ageing and AD progression.

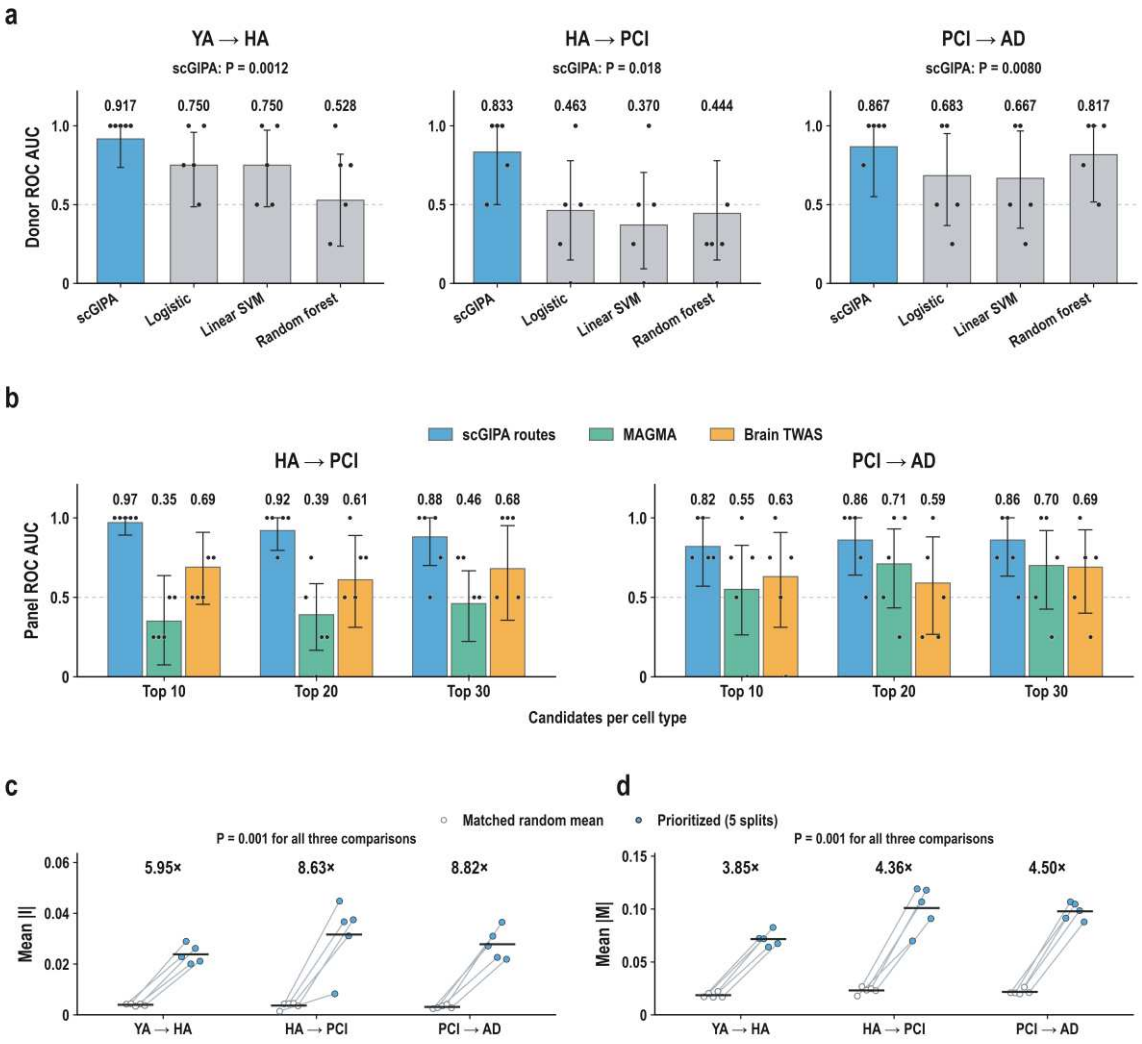


Fig. 2 | Stage discrimination, candidate prioritization and counterfactual attribution by scGIPA. a, Donor-level ROC AUCs for YA to HA, HA to PCI and PCI to AD (17, 15 and 16 donors). Bars show donor-aggregated AUCs, points five partition estimates and error bars donor-bootstrap 95% confidence intervals. P values use one-sided exact donor-label permutations. b, Candidate panels selected in four partitions and evaluated in the fifth. Bars show pooled-record AUCs, points partition AUCs and error bars 95% confidence intervals from 20,000 class-stratified donor-cluster bootstrap resamples. c, Mean |I| from individual expression restoration. d, Mean |M| from individual route masking. In c and d, lines connect matched-random panel means (open circles; 1,000 panels per partition) and prioritized-panel means (blue circles) within each of five validation partitions. Black ticks show across-partition means; labels give prioritized-to-random ratios. Empirical upper-tail P values use plus-one correction. Full statistics are in Supplementary Tables 8–10.

Cellular and functional organization of AD genetic susceptibility across ageing and pathology

To investigate how genes implicated by AD GWAS contribute to biological processes across ageing and pathology, we organized 1,469 AD-associated genes identified by MAGMA into six functional modules using Gene Ontology (GO)-guided annotation (Fig. 3a). Among 235 enriched GO biological process terms, 34 were grouped into six biological themes: organelle and cytoskeletal organization (380 genes), receptor and ERK–MAPK signalling (292 genes), immune regulation (275 genes), endocytosis and intracellular transport (263 genes), lipid efflux and lipoprotein clearance (16 genes), and regulation of amyloid fibril formation (7 genes). Together, these modules comprised 689 distinct genes, more than half of which belonged to multiple modules (359 genes, 52.1%; Fig. 3b and Supplementary Tables 11 and 12). Overlap was particularly pronounced in lipid clearance (87.5%) and amyloid-fibril regulation (100%), while *APOE* belonged to all six modules. This extensive overlap indicates that GWAS-implicated genes participate in interconnected biological programmes rather than independent functional categories, providing a framework for examining how their cellular contributions change across ageing and pathology.

Joint expression restoration further revealed distinct cellular configurations of these programmes across the ageing–pathology sequence (Fig. 3c and Supplementary Table 13). During the transition from young adulthood to healthy ageing, prominent contributions included receptor and ERK–MAPK signalling in microglia, immune and organelle programmes in endothelial cells, and endocytic transport in CA neurons. The transition from healthy ageing to intermediate pathology showed a different configuration, with annotated neural stem cells (NSCs) exhibiting positive contributions across immune regulation, receptor signalling, lipid clearance and amyloid-fibril regulation, alongside prominent endocytic and organelle contributions in neuroblasts. During the transition from intermediate pathology to AD, CA neurons showed prominent contributions across immune, endocytic, receptor and organelle programmes, accompanied by a microglial lipid-clearance contribution. The temporal distribution of contribution strength also differed across programmes. After normalization to each module's maximum across comparisons, endocytosis and intracellular transport retained substantial contributions throughout the three transitions (1.00, 0.89 and 0.93). In contrast, lipid efflux and lipoprotein clearance peaked during early pathology (0.35, 1.00 and 0.84), as did amyloid-fibril regulation (0.37, 1.00 and 0.40). Together, these findings reveal that ageing and pathology involve overlapping functional programmes with distinct temporal profiles and cellular configurations. This raised a further question: do these changing configurations reflect the recruitment of different GWAS-implicated genes, or changes in the cellular and functional contributions of genes contributing across stages?

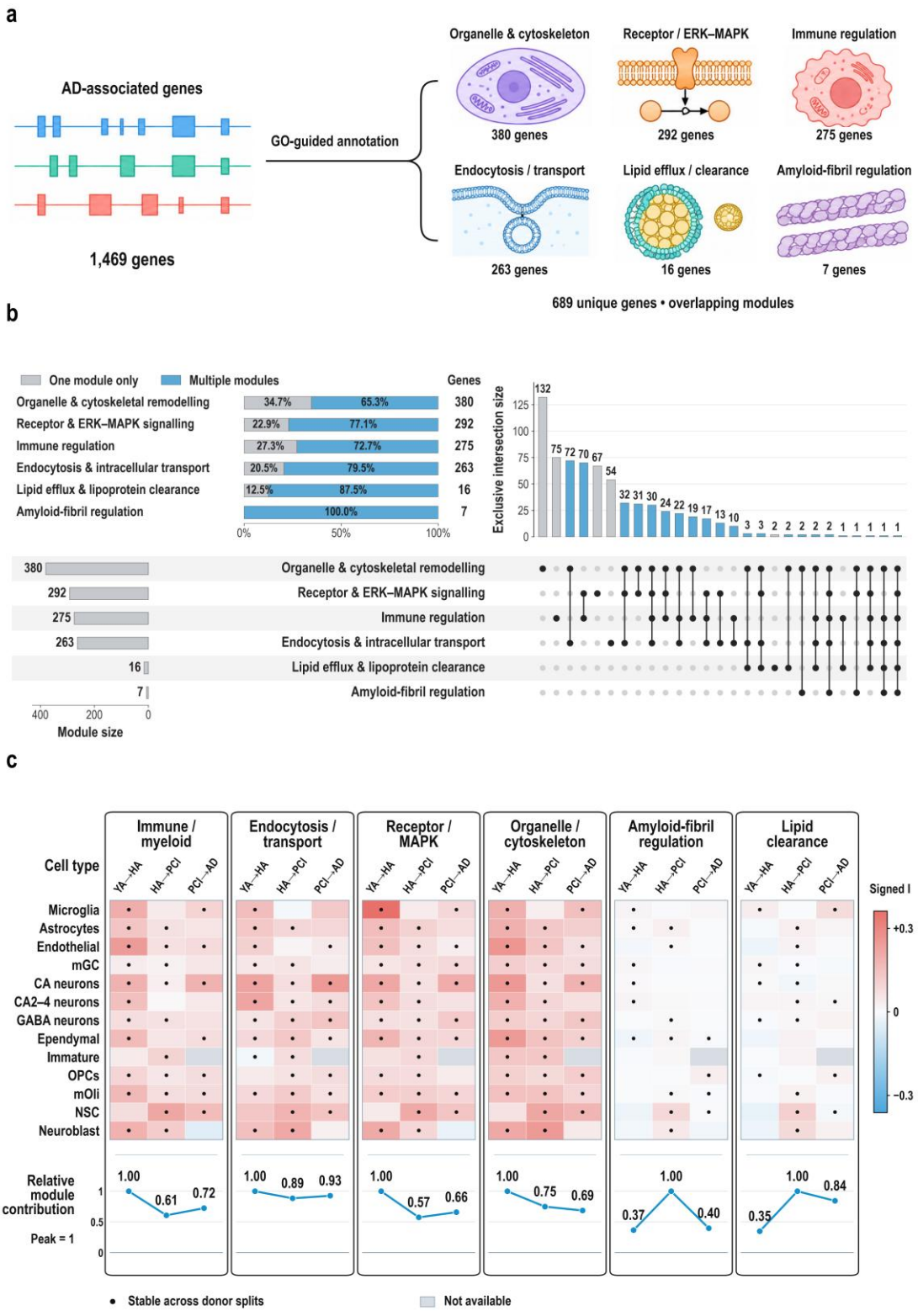


Fig. 3 | Overlapping functional modules show different cellular and stage contributions. a, Definition of six modules from 1,469 AD-associated genes. Of 235 enriched GO biological process terms, 34 were grouped by biological theme using explicit GO identifiers. Module membership is the union of matched intersection genes, yielding 689 unique genes. b, Module-specific proportions of single-module and multiple-module genes, with total module sizes. UpSet bars count genes in each of 27 exact membership combinations, identified by the dot matrix. c, Joint expression-state contributions across 13 cell types and three adjacent comparisons. Heatmaps show signed I averaged equally across evaluable splits. Black dots indicate stable effects in at least three splits with direction consistency of at least 0.80; grey denotes unavailable estimates. Lower profiles show the root-mean-square I across stable cell types, normalized to each module's stage maximum. Definitions, membership and effects are provided in Supplementary Tables 11–13. NSC, annotated neural stem cells; OPC, oligodendrocyte precursor cells; mOli, mature oligodendrocytes; mGC, mature granule cells; CA, hippocampal CA neurons.

Cellular continuity of AD genetic susceptibility across ageing and pathology

To further resolve the stage-dependent organization of AD genetic susceptibility, we examined whether GWAS-implicated genes contributed to ageing, pathology or both. We considered a gene to be participating when its expression made a reproducible contribution to at least one stage comparison in any cell type (stable *I*). Ageing was defined by the YA to HA transition, whereas pathology encompassed HA to PCI or PCI to AD. Among the 1,469 AD-associated genes identified by MAGMA, 461 participated in ageing and 583 in pathology, with 349 contributing to both. The 695 participating genes therefore comprised 112 ageing-only, 234 pathology-only and 349 genes contributing to both ageing and pathology (Fig. 4a and Supplementary Table 14). Genes contributing to both ageing and pathology represented 50.2% of participating genes and 23.8% of all AD-associated genes. A further 662 genes were assessed without stable contributions, while 112 could not be assessed. These classifications reflect reproducible contributions to stage discrimination rather than the presence or absence of gene expression.

Participation in both ageing and pathology extended across all six functional modules, with proportions ranging from 50.7% to 57.2% among participating genes in the four larger modules (Fig. 4b). In the lipid-clearance and amyloid-fibril-regulation modules, eight of nine and four of six participating genes, respectively, contributed to both, although these modules comprised relatively few evaluable genes. Within each cell type, genes contributing to both ageing and pathology accounted for 8.1–22.3% of participating genes, including 68 of 305 in annotated neural stem cells (NSCs), 28 of 148 in microglia and 22 of 190 in CA neurons (Fig. 4c and Supplementary Table 15). Pathology-only contributions predominated in several neuronal and glial populations, whereas ageing-only contributions were relatively prominent in immature neurons and neuroblasts. These findings indicate that a substantial common set of GWAS-implicated genes connects ageing and pathology, although their contributions may occur in different cellular contexts at each stage.

To summarize contribution strength across ageing and pathology, we introduced an ageing–pathology co-participation score (APCS; Fig. 4d). APCS integrates each gene's strongest ageing and pathology contribution percentiles through their harmonic mean, while allowing the contributing cell types and effect directions to differ between stages. APCS had a median of 0.589 for the 349 genes contributing to both ageing and pathology, with *CD2AP* (0.483) and *BIN1* (0.957) illustrating different degrees of co-participation. As a pathology-only comparator, *MS4A4A* had an APCS of 0 because it lacked a stable ageing contribution, indicating that genetic susceptibility genes differ substantially in the strength of their joint involvement across ageing and pathology.

Interestingly, cross-stage co-participation also showed substantial continuity in cellular context. Of the genes contributing to both ageing and pathology, 224 retained a contribution in at least one common cell type, corresponding to 364 shared gene–cell-type pairs. We therefore asked whether this degree of cellular retention exceeded that expected by chance. Using constrained randomization that preserved the overall gene- and cell-type participation structure, the expected number of retained pairs was 284.7 (central 95% null range, 265–304), significantly below the observed 364 pairs (two-sided Monte Carlo $P = 0.0002$; 10,000 randomizations). This enrichment remained when both participation maps were randomized (Supplementary Fig. 1 and Supplementary Table 17). Thus, ageing- and pathology-related contributions showed preferential retention within the same cellular contexts, despite broader redistribution across cell types.

To examine whether this non-random organization of gene contributions extended to an independent dataset, we compared the 349 genes with cell-type-specific co-expression modules reported by Luquez et al.[17] These modules group genes whose expression varies together in the dorsolateral prefrontal cortex, superior temporal gyrus and anterior caudate.

Genes contributing to both ageing and pathology were enriched in microglial ME2, vascular ME1 and oligodendrocyte precursor cell ME1 modules (Supplementary Figs. 2b and 4 and Supplementary Table 16). Microglial ME2 contained 66 of the 318 evaluable genes, including *APOE*, *APOC1*, *TREM2*, *CLU* and *GRN* (1.69-fold enrichment; Benjamini–Hochberg q = 0.00465). These findings show that genes linking ageing and pathology also form coherent expression programmes in independent brain tissue. We next examined the cellular contributions and genetic-route dependence of representative genes.

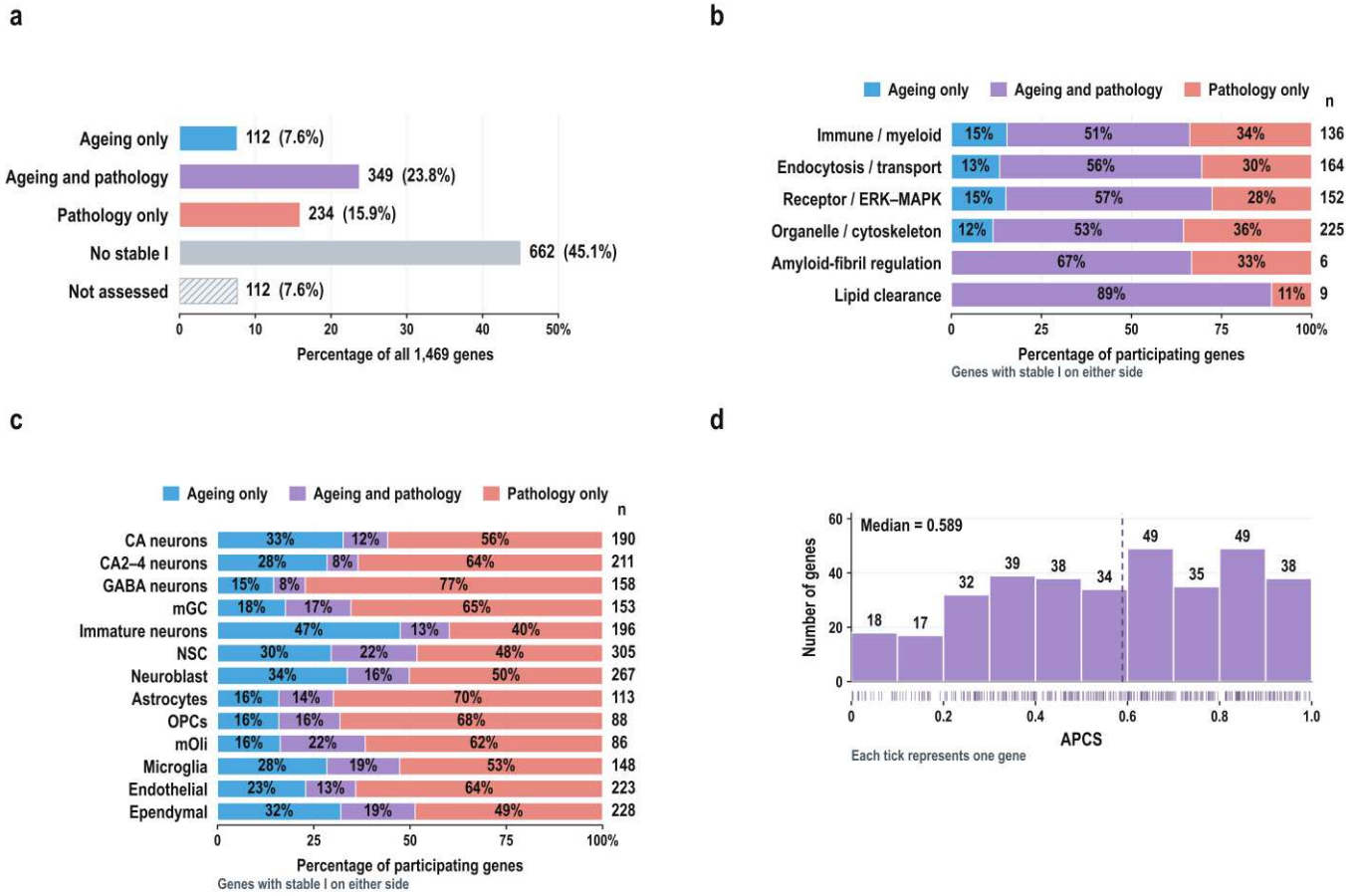


Fig. 4 | Cellular participation across ageing and pathology. a, Stage-participation categories among all 1,469 AD-associated genes. Ageing denotes YA to HA; pathology denotes HA to PCI or PCI to AD. Categories are defined by stable I in the tested comparisons. b, Composition of each functional module using gene-level participation across any cell type. c, Participation classified separately within each cell type. Denominators in b and c include genes with stable I on either side; the adjacent n gives the denominator. Whole-number percentages are rounded. Gene-level co-participation in b may involve different cells, whereas co-participation in c requires the same cell type. d, Ageing–pathology co-participation score (APCS) distribution for all 349 genes contributing to both ageing and pathology, with 0.1-wide bins, individual-gene ticks and the median. APCS combines the strongest ageing and pathology contribution percentiles through their harmonic mean. Complete classifications and scores are provided in Supplementary Tables 14 and 15.

Stage-dependent cellular and genetic contributions of AD susceptibility genes

To further resolve the biological organization of AD genetic susceptibility, we examined representative ageing-only genes, pathology-only genes and genes contributing to both, considering their cellular contexts, expression-state contributions and genetic-route dependence. Among ageing-only genes, *PVR* and *HBEGF* showed stable expression-state contributions in endothelial cells during the YA to HA transition (I = +0.0348 and +0.0030, respectively; Fig. 5a), without stable contributions during either pathological transition. *PVR* also exhibited stable but oppositely directed genetic-route dependence (*M* = −0.0220), whereas no evaluable endothelial route was available for *HBEGF*. These observations place endothelial-associated expression changes within the ageing component of AD genetic susceptibility. The established roles of *PVR* in endothelial leukocyte passage and *HBEGF* in pericyte recruitment and vascular stabilization provide a biological context for these contributions,[18,19] suggesting that genes associated with AD susceptibility may participate in vascular homeostatic processes before the emergence of overt pathology. Observed endothelial *PVR* expression was lower in HA than in YA (Fig. 5b).

Pathology-only genes revealed distinct immune and neuronal configurations. *CD33*, a microglial receptor implicated in inhibition of amyloid-β uptake,[20] showed stable contributions specifically during PCI to AD, with concordant positive *I* (+0.0030) and *M* (+0.0068) in microglia. By contrast, *MS4A4A*, a regulator of soluble *TREM2*,[21] contributed across both pathological transitions within the same microglial context, but its expression-state contribution changed direction from HA to PCI (*I* = −0.0045) to PCI to AD (*I* = +0.0154), accompanied by stable negative genetic-route dependence in the latter transition (*M* = −0.0727). A parallel pattern emerged in neurons: *FERMT2*, previously linked to APP-dependent axonal and synaptic functions,[22] showed opposing expression-state contributions in CA2–4 neurons during early and later pathology (*I* = −0.0045 and +0.0045, respectively). Together, these examples indicate that pathology-associated contributions may emerge at particular stages or change direction within a retained cellular context. Microglial *CD33* expression was higher in AD (Fig. 5b).

APOE, *CLU* and *BIN1* contributed to both ageing and pathology, with different dominant cell types across stages. *APOE*, a central AD susceptibility gene involved in lipid metabolism, showed strong co-participation across ageing and pathology (APCS = 0.984). Its dominant expression-state contribution occurred in annotated neural stem cells during ageing and early pathology (*I* = −0.0332 and +0.0556), before shifting to oligodendrocyte precursor cells during later pathology (*I* = −0.0048). *CLU* showed a related but distinct configuration (APCS = 0.942), with its dominant endothelial contributions during ageing and early pathology (*I* = +0.0129 and +0.0402), followed by a larger oligodendrocyte precursor cell contribution during PCI to AD (*I* = +0.0365), while a smaller endothelial contribution persisted. Notably, *CLU* retained positive expression-state contributions while its stable *M* values differed between ageing endothelial cells (*M* = +0.1719) and later-pathology oligodendrocyte precursor cells (*M* = −0.0902). These patterns illustrate how genes contributing to both ageing and pathology may connect vascular and glial cellular contexts without maintaining identical expression-state or regulatory contributions across stages. *APOE* expression in annotated NSCs peaked in HA and declined in PCI (Fig. 5b). Additional *APOE* contexts are shown in Supplementary Fig. 2a. Observed expression for the remaining representative contexts is shown in Supplementary Fig. 3.

BIN1 showed strong co-participation across ageing and pathology (APCS = 0.957). Its dominant expression-state contribution shifted from microglia during ageing (I = +0.0284) to mature oligodendrocytes during early pathology (I = +0.0104) and back to microglia during later pathology (I = +0.0156). Within microglia, expression-state contributions remained reproducibly positive across all three comparisons, whereas stable genetic-route dependence changed from negative during ageing (M = −0.0932) to positive during early pathology (M = +0.0767) and negative during later pathology (M = −0.0603). Thus, *BIN1* retained a microglial expression-state contribution while its associated genetic-route dependence changed across stages. Together, these genes support a working model in which ageing-associated vascular contributions and pathology-associated immune and neuronal responses are linked by genes contributing to both, with changing cellular contributions and genetic-route dependence within a common neurovascular environment (Fig. 6).

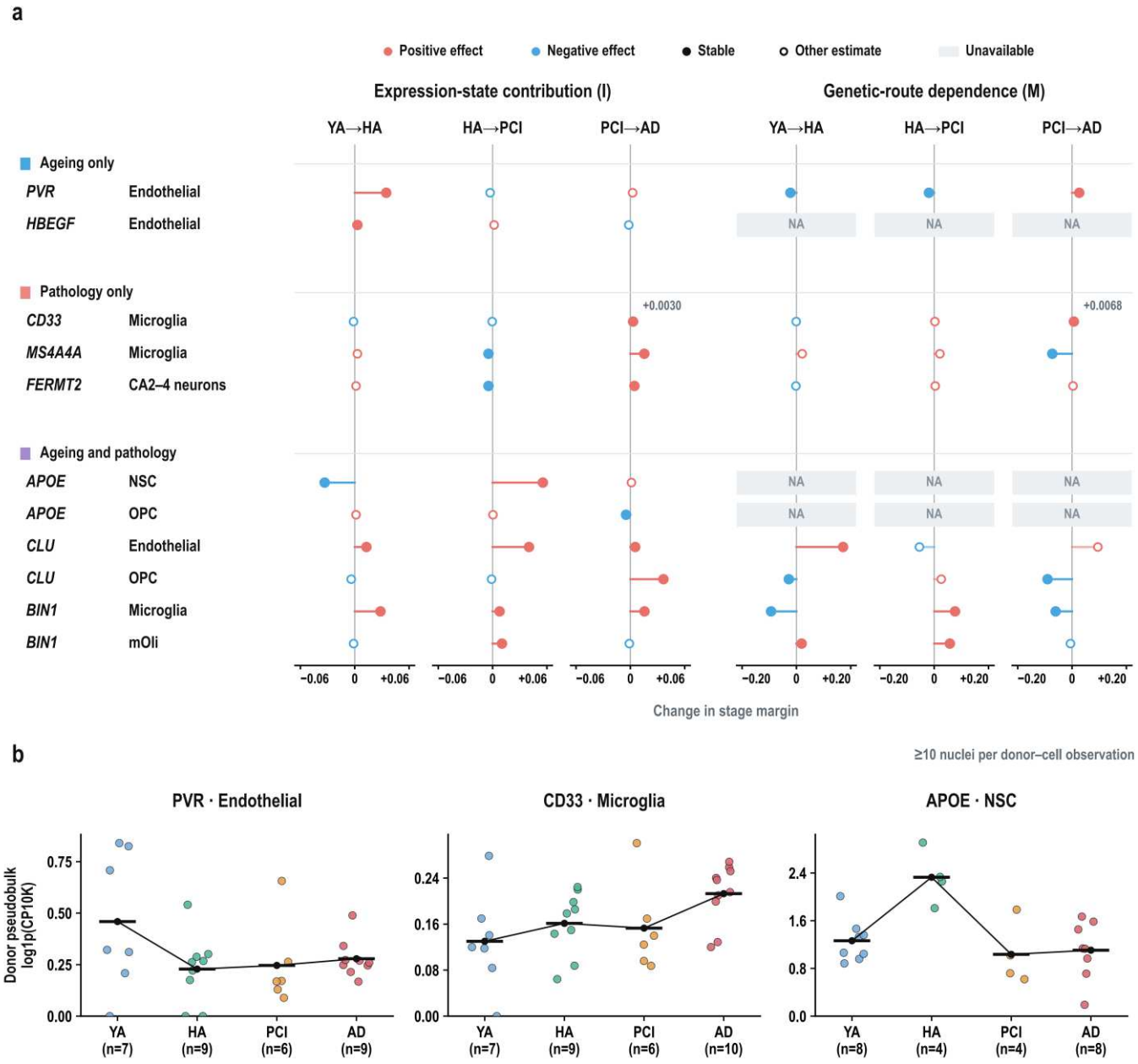


Fig. 5 | Expression-state contributions and genetic-route dependence across stages. a, Expression-state contribution (I, left) and genetic-route dependence (M, right) for 11 representative gene–cell contexts across three adjacent-stage comparisons. Genes are grouped by stable I in ageing only, pathology only, or both. Horizontal positions show the change in the later-versus-earlier logit margin after restoring expression to the same-cell-type reference from the preceding stage (I) or masking the corresponding genetic input (M), calculated as original minus perturbed. Positive effects are coral and negative effects blue; signs describe perturbation effects rather than expression changes. Filled circles indicate I meeting reproducibility criteria or M reaching at least 80% directional agreement across 15 models (five partitions and three initializations). Open circles show other available estimates; grey NA marks unavailable estimates. The I columns share one scale, and M columns share a separate scale. b, Observed expression for PVR in endothelial cells, CD33 in microglia and APOE in annotated neural stem cells (NSCs). Each point represents a donor with at least ten nuclei of the indicated cell type; expression is log1p(CP10K). Black bars and connecting lines indicate means of independent stage groups, with donor counts shown. Observed expression for the remaining eight representative contexts is shown in Supplementary Fig. 3. Additional APOE contexts and external co-expression support are shown in Supplementary Fig. 2. OPC, oligodendrocyte precursor cells; mOli, mature oligodendrocytes.

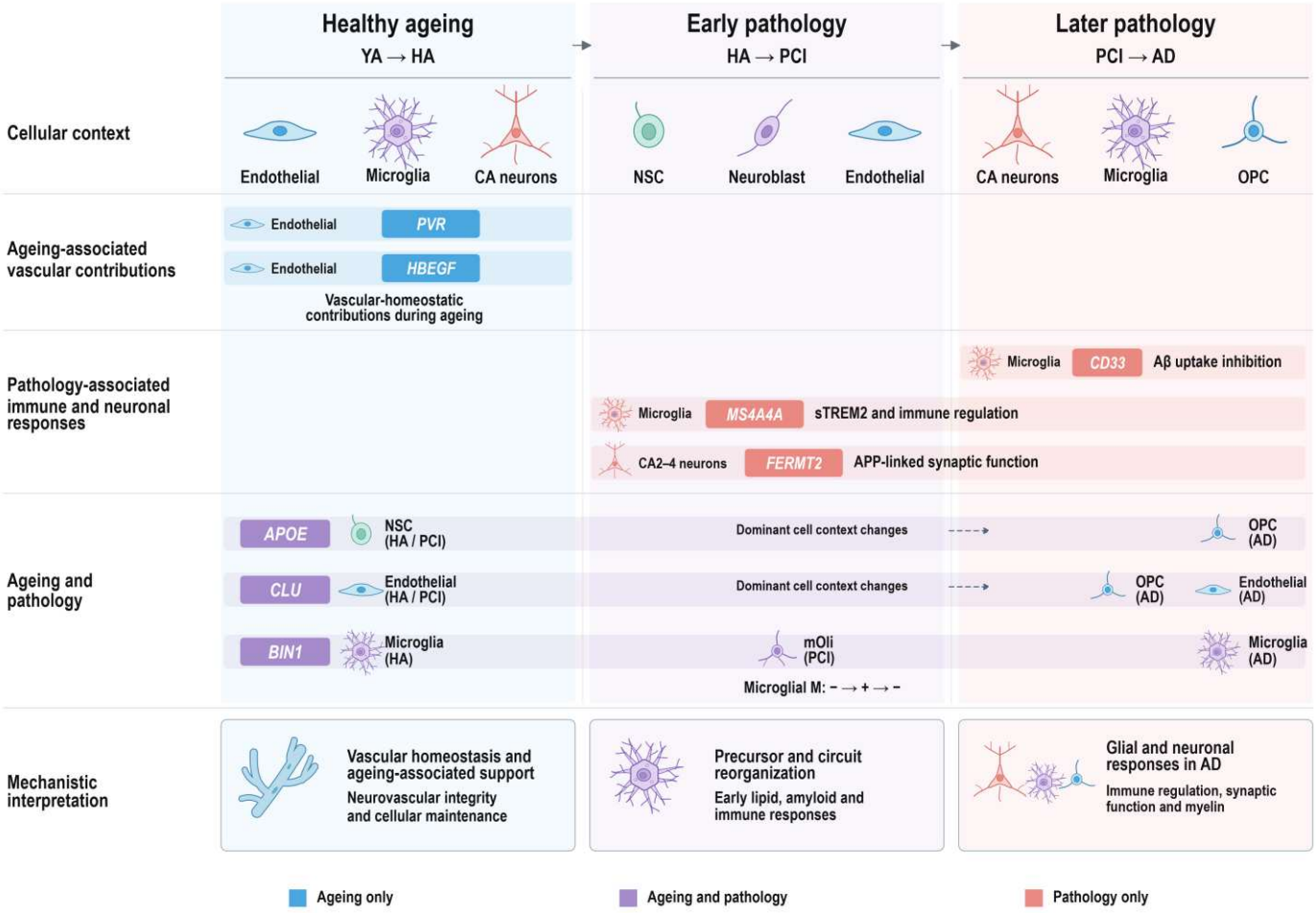


Fig. 6 | A working model of stage-dependent AD genetic susceptibility within a shared neurovascular environment. Columns show healthy ageing (YA to HA), early pathology (HA to PCI) and later pathology (PCI to AD). Endothelial PVR and HBEGF link the ageing findings to leukocyte passage and pericyte support; CD33, MS4A4A and FERMT2 link pathological contributions to amyloid uptake, TREM2 regulation and APP-dependent synaptic functions.[18,19,20,21,22] The rows for genes contributing to both ageing and pathology show selected cell types with dominant I contributions for APOE, CLU and BIN1. Smaller endothelial CLU contributions and recurrent microglial BIN1 contributions accompany the highlighted OPC and mature oligodendrocyte contributions. The BIN1 M sequence refers to microglia across healthy ageing, early pathology and later pathology (negative, positive and negative, respectively). Coloured bands mark stage participation; cells on each band show the corresponding cellular contexts. The bottom row presents the proposed connections between vascular maintenance, early precursor and circuit responses, and later glial and neuronal responses within a shared neurovascular environment. NSC, annotated neural stem cells; OPC, oligodendrocyte precursor cells; mOli, mature oligodendrocytes.

Discussion

Our study provides a multidimensional view of how genes implicated by Alzheimer disease (AD) GWAS contribute to cellular changes across healthy ageing and pathological progression. By integrating genetic associations, brain regulatory evidence and hippocampal single-nucleus transcriptomes, scGIPA enabled us to examine these dimensions within a common framework. We found that AD-associated genes participate in overlapping functional programmes whose cellular contributions vary across ageing and pathology. Notably, half of the genes with reproducible contributions participated in both ageing and pathology, yet their cellular contexts and dependence on genetically informed regulatory inputs were not necessarily conserved. These findings support a view of AD genetic susceptibility as dynamically organized across the ageing–pathology continuum, in which persistent genetic participation coexists with changes in cellular and functional contributions.

A central finding was the substantial genetic continuity between healthy ageing and AD pathology. A large proportion of genes with reproducible expression-state contributions contributed to both ageing and pathological transitions, and this overlap extended across all six functional modules. Importantly, participation in both ageing and pathology did not imply that genes acted through identical cellular contexts at each stage. Instead, many genes retained at least one common cellular context while also showing stage-dependent redistribution across cell types. Enrichment in external microglial, vascular and oligodendrocyte precursor cell co-expression modules further supported the biological organization of this gene set.[17] At the functional level, this continuity was accompanied by marked temporal reorganization. Endocytosis and intracellular transport remained prominent across the ageing–pathology continuum, suggesting a persistent role for intracellular trafficking, whereas lipid efflux and lipoprotein clearance and regulation of amyloid fibril formation became most prominent during early pathology. This stage was also characterized by stronger contributions from annotated neural stem cells and neuroblasts, followed by greater neuronal and microglial involvement during later pathology. Together, these findings suggest that ageing and AD pathology share a common genetic substrate whose cellular and functional deployment is progressively reorganized, with early pathology representing a distinct transitional state marked by shifts in lipid handling, amyloid-related processes and cellular maintenance rather than simply an intermediate form of clinical AD. Human single-cell studies have likewise resolved coordinated cellular trajectories across ageing and AD,[23] disease-stage-specific microglial states,[24] and transient early-pathology responses.[25]

Representative genes helped place these broader patterns into a biological context. The ageing-associated endothelial contributions of *PVR* and *HBEGF* suggest a connection between AD susceptibility and vascular processes during healthy ageing.[26] Hippocampal barrier integrity and blood–brain transport change with ageing, and APOE4 links vascular dysfunction to cognitive decline.[27,28,29] In contrast, *CD33*, *MS4A4A* and *FERMT2* illustrated pathology-associated contributions involving microglial immune responses and neuronal functions. Genes contributing to both ageing and pathology provided a link between these configurations. *APOE* showed prominent contributions in annotated neural stem cells during ageing and early pathology, followed by oligodendrocyte precursor cells during later pathology. *CLU* connected endothelial contributions during ageing and early pathology with later oligodendrocyte precursor cell involvement, whereas *BIN1* showed changing contributions across microglial and oligodendrocyte contexts. Experimental studies connect APOE to oligodendroglial cholesterol handling and microglial lipid accumulation,[30,31] and CLU to vascular amyloid clearance and OPC differentiation and myelination.[32,33,34] *BIN1* is expressed in mature oligodendrocytes,[35] and an AD-associated enhancer regulates its expression in microglia.[36] These examples illustrate an important distinction: participation of the same susceptibility gene across stages does not necessarily imply that its cellular contribution or regulatory dependence remains unchanged. These observations collectively support a working model in which AD genetic susceptibility is organized through interconnected vascular, glial and neuronal programmes within a shared neurovascular environment (Fig. 6). Ageing-associated changes at vascular interfaces could alter the extracellular conditions in which glial and neuronal responses develop, potentially linking vascular maintenance to lipid handling, amyloid-related processes and neuronal support. In this context, susceptibility genes contributing to both ageing and pathology may connect biological processes that become prominent at different stages, even as their cellular contributions change. This model does not establish a linear sequence in which vascular alterations initiate subsequent immune and neuronal dysfunction. Rather, it highlights the possibility that ageing and AD pathology involve a common set of susceptibility genes expressed through changing interactions among vascular, glial and neuronal environments. Spatially resolved studies and cell-type-specific perturbations will be important for testing these proposed relationships.

As GWAS and post-GWAS analyses increasingly connect disease-associated loci to candidate genes and regulatory contexts,[37] an important next step is to understand how these associations relate to changing cellular states during ageing and disease progression.[38] scGIPA addresses this challenge by distinguishing expression-state contribution from dependence on genetically informed regulatory inputs. The opposing responses of these two readouts for endothelial *PVR* during ageing and *APOE* during early pathology illustrate how expression-state and regulatory contributions can differ within the same gene–cell context. Together with the changing cellular contributions and genetic-route dependence observed for *BIN1* and *CLU*, these findings show why genetic susceptibility cannot be fully understood from gene expression, cellular localization or genetic association alone. Although the counterfactual readouts do not establish causal effects, scGIPA provides a framework for investigating how genetically implicated genes contribute across cellular states and disease stages. With suitable genetic, regulatory and single-cell data, this approach could also be extended to other complex diseases.

In conclusion, our findings extend the interpretation of AD genetic susceptibility beyond identifying associated genes and cell types towards understanding how their contributions are organized across ageing and pathology. The coexistence of gene participation in both ageing and pathology and changing cellular and regulatory contributions suggests that inherited susceptibility is expressed through an interconnected but progressively reorganized cellular landscape. This perspective provides a basis for investigating how ageing-associated processes relate to the emergence and progression of AD pathology.

Methods

Data and expression processing

We analysed released human hippocampal single-nucleus RNA-sequencing data (GSE268609), using the source annotations for 131,869 nuclei from 33 donors: 8 young adults (YA), 9 healthy aged individuals (HA), 6 with preclinical intermediate pathology (PCI) and 10 with Alzheimer's disease (AD). SuperAgers were excluded. Thirteen cell types were compared across YA–HA, HA–PCI and PCI–AD. Ensembl identifiers were mapped to GENCODE gene symbols. Counts were normalized to 10,000 per nucleus and log1p-transformed. Donor–cell-type pseudobulks summed counts from at least ten nuclei and underwent the same normalization. Donors were weighted equally within each group and cell type. [14]

Ethics statement

This study reanalysed publicly available human hippocampal single-nucleus data (GSE268609) and involved no new recruitment or tissue collection. In the original study, the YA, HA, PCI and AD samples came from the University of Washington repository. The original study reports informed consent for tissue collection and a determination by the University of Washington Institutional Review Board that the post-mortem repository work did not constitute human subjects research.[14]

Genetic and regulatory evidence

AD GWAS summary statistics (GCST90704646) were analysed using MAGMA v1.10, European 1000 Genomes linkage disequilibrium (LD), gene bodies extended by 10 kb and variant-specific effective sample sizes. The 1,469 AD-associated genes with Benjamini–Hochberg false discovery rate (FDR) below 0.05 formed the analysis background. Cell-expression specificity was tested as a continuous MAGMA gene property. [1,39,40]

Cell-specific regulatory inputs combined SingleBrain cell-type-specific cis-eQTL associations and GWAS signals (both $P \leq 10^{-3}$), using direct variant overlap or allele-harmonized LD proxies ($r^2 \geq 0.8$). BrainMeta cortical cis-eQTLs supplemented cell types lacking SingleBrain coverage. Signed association scores incorporated aligned GWAS/eQTL directions and, for proxies, signed LD. Direct and proxy gene scores were the sign of the mean link score multiplied by the square root of its largest absolute magnitude; proxy magnitudes also incorporated absolute LD correlation. Bulk-cortex scores were the mean signed score multiplied by 0.35. Scores were weighted by evidence source (direct, 1.0; proxy, 0.8; bulk cortex, 0.4), MAGMA evidence and cell-property enrichment. Gene and cell multipliers were $1+\max(0,Z)/8$ and $1+\max(0,\beta)/\max_c \max(0,\beta_c)$, respectively. Duplicate gene–cell-type entries retained the largest absolute weighted value. Within each cell type, nonzero priors were divided by their 95th absolute-value percentile and clipped to [−4,4]. The matrix contained 3,087 nonzero regulatory inputs across 1,011 genes. [15,16]

scGIPA and donor validation

scGIPA combines a variational expression encoder, a learned cell-type embedding and a regulatory branch receiving $x \odot P_c$, where x is expression and P_c the cell-specific genetic prior. Their 48-dimensional representations are added for expression reconstruction and four-group classification. The expression encoder has two 384-unit layers; the regulatory branch and classifier each have a 192-unit hidden layer. Hidden layers use GELU activation. Layer normalization is applied in the expression encoder, regulatory branch and decoder; 0.1 dropout follows the encoder's first hidden layer and is used in the decoder and classifier. A separate head predicts ordinal pathology (HA=0, PCI=1, AD=2) from the expression latent; YA contributes to reconstruction and classification only.

The objective combines reconstruction mean-squared error, classification cross-entropy, ordinal-stage error, variational divergence and expression-direction anchoring, weighted 1, 1, 0.2, 0.001 and 0.2. Anchoring aligns decoded regulatory responses with adjacent-stage expression differences in training-donor pseudobulks. Models were fitted for 25 epochs using AdamW (learning rate 2×10^{-4}; weight decay 10^{-4}; batch size 128), balanced group sampling and gradient clipping at 5. Five donor partitions with three initializations each yielded 15 models. Validation donors were excluded from parameter fitting and training-reference calculation within each partition. Donors could recur across partitions, so evaluation used repeated donor-validation partitions.

Estimation of I and M

For adjacent stages a and b, the stage margin s_{ab} is the classifier logit for b minus that for a. Let x be a target-stage validation donor's expression profile in cell type c and $r = x \odot P_c$ its genetic regulatory input. Expression restoration replaces all columns of gene g with the preceding-stage training-donor mean in the same cell type, producing x_{rest} and $r_{rest} = x_{rest} \odot P_c$. Genetic-input masking sets that gene's entries in r to zero, producing r_{mask} while holding x and its expression representation fixed. The two readouts are:

$$I_{g,c}^{a\to b} = \langle s_{ab}(x,r) - s_{ab}(x_{rest}, r_{rest})\rangle_d \qquad (1)$$

$$M_{g,c}^{a\to b} = \langle s_{ab}(x,r) - s_{ab}(x, r_{mask})\rangle_d \qquad (2)$$

Angle brackets denote equal averaging over eligible target-stage donors within a model. At least two reference donors and one target donor were required. Inference used posterior means with fixed parameters. Both branches were recalculated for expression restoration; genetic-input masking preserved the expression branch. Positive I or M indicates that the perturbation reduces the stage margin; negative values indicate an increase. Supplementary Methods give the model and aggregation definitions.

An I estimate was retained within a partition with at least two initialization estimates and directional agreement ≥2/3. Reproducible single-gene I required at least three retained partitions, ≥0.80 agreement across partitions and an absolute equally weighted mean reaching the 90th percentile of eligible absolute partition effects: 0.0023816 for ageing and 0.0024491 for pathology. The two pathology comparisons were pooled to estimate their threshold. Representative-gene M used the mean of available model estimates with ≥0.80 directional agreement. Unavailable estimates and available estimates below reproducibility criteria were labelled separately.

Discrimination and candidate benchmarks

Stage margins were averaged across available cell types and initializations, then across validation appearances, giving one score per donor. ROC AUC confidence intervals used 10,000 class-stratified donor bootstrap resamples; one-sided exact label permutations preserved group counts. Logistic regression, linear support vector machines, random forests and expression-centroid comparators used the same donor partitions. PCA-based comparators used training-derived cell-type centring, standardization and up to 20 principal components.

For candidate-panel comparisons, genes were ranked within each cell type by absolute median M across four partitions, requiring directional agreement ≥0.75. Panels of 10, 20 or 30 candidates were evaluated in the omitted partition. MAGMA and brain S-PrediXcan panels matched their cell types and feature counts. A common standardized, balanced logistic classifier (C=0.1) evaluated donor expression features. Panel AUCs pooled validation prediction records, with 20,000 class-stratified donor-cluster bootstrap resamples. [41,42]

Individual I and M benchmarks ranked genes by the corresponding absolute median I or M across the other four partitions, requiring directional agreement ≥0.75, and evaluated ten candidates per cell type in the omitted partition. Each benchmark used 1,000 random panels matched for cell type and feature count. Additional matching used training expression and expression-reset magnitude for I, and expression and prior magnitude for M, sampling from the 30 nearest eligible candidates. Effects were averaged across initializations before taking absolute values, then averaged equally across partitions. Empirical upper-tail P values used the plus-one correction.

Functional modules and gene participation

Among 235 Gene Ontology biological-process terms enriched in the AD-associated genes, 34 were grouped by biological theme into six functional modules. Each module comprised the union of its enrichment-intersection genes, allowing membership in multiple modules. GO identifiers, adjusted P values and memberships are provided in Supplementary Tables 11 and 12. Module I jointly reset all represented member genes; module M jointly masked their nonzero regulatory inputs. Reproducibility used the partition and directional criteria above, without the single-gene magnitude threshold. Stage profiles used root-mean-square I across reproducible cell types, normalized to each module's maximum across comparisons. [43,44]

A gene participated in ageing if it had reproducible YA–HA I in any cell type, and in pathology if it had reproducible I in either pathology comparison. These criteria defined ageing-only genes, pathology-only genes and genes contributing to both and were also applied separately within each cell type. APCS was the harmonic mean of each gene's strongest reproducible absolute-I percentile in ageing (A) and pathology (P), ranked within each comparison:

$$\mathrm{APCS} = \frac{2AP}{A+P} \qquad (3)$$

APCS was set to zero when either qualifying contribution was absent. APCS ranked the 349 genes contributing to both ageing and pathology, allowing cell type and effect direction to differ between ageing and pathology.

Cell-type overlap and external co-expression

Same-cell-type overlap was tested for the 349 genes contributing to both ageing and pathology across jointly evaluable gene–cell-type pairs. With the ageing map fixed, reversible 2×2 switches randomized pathology assignments while preserving each gene's number of participating cell types, each cell type's gene count and unavailable positions. Four chains provided 10,000 saved randomizations after 100,000 burn-in proposals, with 2,000 proposals between saved states. The two-sided Monte Carlo P value was twice the smaller inclusive tail, with plus-one correction and a maximum of one. A sensitivity analysis independently randomized both maps. Input maps, overlap summaries and chain diagnostics are provided in Supplementary Table 17.

External enrichment used Luquez et al.'s published cell-type co-expression modules. Eligible backgrounds comprised AD-associated genes with external assignments and available discovery expression. Random sets matched counts of genes contributing to both ageing and pathology within discovery-expression quintiles and external cell-class coverage strata. External cell-class coverage is the number of external cell classes with a non-missing module annotation for each gene. For each of 93 eligible modules, 10,000 random sets yielded an upper-tail empirical P value; Benjamini–Hochberg correction covered all 93 tests. Enrichment was observed overlap divided by its null mean. [17]

Representative genes illustrated ageing-only, pathology-only and ageing-and-pathology contributions. Observed expression plots used equally weighted donor pseudobulks. Donors were the units of expression summaries and discrimination; model initializations and partitions assessed contribution reproducibility.

Funding

This work was supported by the National Natural Science Foundation of China (62622309 and 62472120 (Tao Jiang), 82604006 (Yingchao Song), and 32670828 (Xiao Chang)), the National Key Research and Development Program of China (2024YFC3406303 (Tao Jiang)), the Fundamental Research Funds for the Central Universities (XNJKKGYDJ2026010 (Tao Jiang)), the Harbin Institute of Technology Kunpeng & Ascend Center of Cultivation (Tao Jiang), and the Shandong Provincial Natural Science Foundation (ZR2026QC0955 (Yingchao Song)).

Author contributions

Z.M. conducted the research, analysed the data and drafted the manuscript. Y.S. and X.W. curated the data and reviewed the manuscript. M.B., S.W., Z.C. and X.M. contributed to manuscript review and revision. T.J., X.C. and T.X. supervised the study and revised the manuscript. All authors reviewed and approved the final manuscript.

Competing interests

The authors declare no competing interests.

Data availability

Hippocampal data are available under GEO accession GSE268609 and GWAS summary statistics under accession GCST90704646. Regulatory and external co-expression data are available from the cited SingleBrain, BrainMeta and Luquez studies. Supplementary Tables 1–17 provide gene sets, module definitions, contribution estimates and supplementary validation results.

Code availability

Source code for scGIPA, including model training, I/M estimation and a runnable synthetic example, is publicly available at https://github.com/ziangmeng/scGIPA.

References

1. EADB, EADI, Bonn, ADGC, CHARGE, FinnGen, GERAD, GR@ACE/DEGESCO and PGC-ALZ consortia. Consensus meta-analysis of genome-wide association studies for Alzheimer's disease and related dementias. Nature Genetics 58, 1214–1225 (2026). https://doi.org/10.1038/s41588-026-02583-1

2. De Strooper, B. and Karran, E. Inflection points and transitions in Alzheimer's disease. Nature (2026). https://doi.org/10.1038/s41586-026-11110-5

3. Lu, A., Chen, W.-T., Dalby, M. et al. Human microglial transitions at the Aβ–tau inflection point associate with divergent pathways to dementia and resilience. Nature Medicine 32, 2047–2059 (2026). https://doi.org/10.1038/s41591-026-04393-8

4. Mathys, H. et al. Single-cell multiregion dissection of Alzheimer's disease. Nature 632, 858–868 (2024). https://doi.org/10.1038/s41586-024-07606-7

5. Mathys, H. et al. Single-cell transcriptomic analysis of Alzheimer's disease. Nature 570, 332–337 (2019). https://doi.org/10.1038/s41586-019-1195-2

6. Morabito, S., Miyoshi, E., Michael, N. et al. Single-nucleus chromatin accessibility and transcriptomic characterization of Alzheimer's disease. Nature Genetics 53, 1143–1155 (2021). https://doi.org/10.1038/s41588-021-00894-z

7. Bryois, J., Calini, D., Macnair, W. et al. Cell-type-specific cis-eQTLs in eight human brain cell types identify novel risk genes for psychiatric and neurological disorders. Nature Neuroscience 25, 1104–1112 (2022). https://doi.org/10.1038/s41593-022-01128-z

8. Zhang, M. J., Hou, K., Dey, K. K. et al. Polygenic enrichment distinguishes disease associations of individual cells in single-cell RNA-seq data. Nature Genetics 54, 1572–1580 (2022). https://doi.org/10.1038/s41588-022-01167-z

9. Zhang, S. et al. Single-cell polygenic risk scores dissect cellular and molecular heterogeneity of complex human diseases. Nature Biotechnology 44, 845–861 (2026). https://doi.org/10.1038/s41587-025-02725-6

10. Lopez, R., Regier, J., Cole, M. B., Jordan, M. I. and Yosef, N. Deep generative modeling for single-cell transcriptomics. Nature Methods 15, 1053–1058 (2018). https://doi.org/10.1038/s41592-018-0229-2

11. Lotfollahi, M., Wolf, F. A. and Theis, F. J. scGen predicts single-cell perturbation responses. Nature Methods 16, 715–721 (2019). https://doi.org/10.1038/s41592-019-0494-8

12. Roohani, Y., Huang, K. and Leskovec, J. Predicting transcriptional outcomes of novel multigene perturbations with GEARS. Nature Biotechnology 42, 927–935 (2024). https://doi.org/10.1038/s41587-023-01905-6

13. Cui, H., Wang, C., Maan, H. et al. scGPT: toward building a foundation model for single-cell multi-omics using generative AI. Nature Methods 21, 1470–1480 (2024). https://doi.org/10.1038/s41592-024-02201-0

14. Disouky, A. et al. Human hippocampal neurogenesis in adulthood, ageing and Alzheimer's disease. Nature 652, 1264–1273 (2026). https://doi.org/10.1038/s41586-026-10169-4

15. Jang, B. et al. A meta-analysis of single-nucleus expression quantitative trait loci linking genetic risk to brain disorders. Nature Genetics 58, 737–747 (2026). https://doi.org/10.1038/s41588-026-02541-x

16. Qi, T. et al. Genetic control of RNA splicing and its distinct role in complex trait variation. Nature Genetics 54, 1355–1363 (2022). https://doi.org/10.1038/s41588-022-01154-4

17. Luquez, T., Algoo, J., Chiu, R. et al. Cell-type signatures of Alzheimer's disease shared across population groups. Nature 657, 191–201 (2026). https://doi.org/10.1038/s41586-026-10793-0

18. Reymond, N. et al. DNAM-1 and PVR regulate monocyte migration through endothelial junctions. Journal of Experimental Medicine 199, 1331–1341 (2004). https://doi.org/10.1084/jem.20032206

19. Stratman, A. N., Schwindt, A. E., Malotte, K. M. and Davis, G. E. Endothelial-derived PDGF-BB and HB-EGF coordinately regulate pericyte recruitment during vasculogenic tube assembly and stabilization. Blood 116, 4720–4730 (2010). https://doi.org/10.1182/blood-2010-05-286872

20. Griciuc, A. et al. Alzheimer's disease risk gene CD33 inhibits microglial uptake of amyloid beta. Neuron 78, 631–643 (2013). https://doi.org/10.1016/j.neuron.2013.04.014

21. Deming, Y. et al. The MS4A gene cluster is a key modulator of soluble TREM2 and Alzheimer's disease risk. Science Translational Medicine 11, eaau2291 (2019). https://doi.org/10.1126/scitranslmed.aau2291

22. Eysert, F. et al. Alzheimer's genetic risk factor FERMT2 (Kindlin-2) controls axonal growth and synaptic plasticity in an APP-dependent manner. Molecular Psychiatry 26, 5592–5607 (2021). https://doi.org/10.1038/s41380-020-00926-w

23. Green, G. S., Fujita, M., Yang, H.-S. et al. Cellular communities reveal trajectories of brain ageing and Alzheimer's disease. Nature 633, 634–645 (2024). https://doi.org/10.1038/s41586-024-07871-6

24. Sun, N., Victor, M. B., Park, Y. P. et al. Human microglial state dynamics in Alzheimer's disease progression. Cell 186, 4386–4403.e29 (2023). https://doi.org/10.1016/j.cell.2023.08.037

25. Gazestani, V., Kamath, T., Nadaf, N. M. et al. Early Alzheimer's disease pathology in human cortex involves transient cell states. Cell 186, 4438–4453.e23 (2023). https://doi.org/10.1016/j.cell.2023.08.005

26. Yang, A. C., Vest, R. T., Kern, F. et al. A human brain vascular atlas reveals diverse mediators of Alzheimer's risk. Nature 603, 885–892 (2022). https://doi.org/10.1038/s41586-021-04369-3

27. Montagne, A., Barnes, S. R., Sweeney, M. D. et al. Blood-brain barrier breakdown in the aging human hippocampus. Neuron 85, 296–302 (2015). https://doi.org/10.1016/j.neuron.2014.12.032

28. Yang, A. C., Stevens, M. Y., Chen, M. B. et al. Physiological blood–brain transport is impaired with age by a shift in transcytosis. Nature 583, 425–430 (2020). https://doi.org/10.1038/s41586-020-2453-z

29. Montagne, A. et al. APOE4 leads to blood–brain barrier dysfunction predicting cognitive decline. Nature 581, 71–76 (2020). https://doi.org/10.1038/s41586-020-2247-3

30. Blanchard, J. W. et al. APOE4 impairs myelination via cholesterol dysregulation in oligodendrocytes. Nature 611, 769–779 (2022). https://doi.org/10.1038/s41586-022-05439-w

31. Haney, M. S. et al. APOE4/4 is linked to damaging lipid droplets in Alzheimer's disease microglia. Nature 628, 154–161 (2024). https://doi.org/10.1038/s41586-024-07185-7

32. Wojtas, A. M., Kang, S. S., Olley, B. M. et al. Loss of clusterin shifts amyloid deposition to the cerebrovasculature via disruption of perivascular drainage pathways. Proceedings of the National Academy of Sciences of the United States of America 114, E6962–E6971 (2017). https://doi.org/10.1073/pnas.1701137114

33. Beiter, R. M., Raghavan, T. P., Suchocki, O. et al. Clusterin induced by OPC phagocytosis blocks IL-9 secretion to inhibit myelination in a model of Alzheimer's disease. Heliyon 11, e41635 (2025). https://doi.org/10.1016/j.heliyon.2025.e41635

34. Liu, Z., Chao, J., Wang, C. et al. Astrocytic response mediated by the CLU risk allele inhibits OPC proliferation and myelination in a human iPSC model. Cell Reports 42, 112841 (2023). https://doi.org/10.1016/j.celrep.2023.112841

35. De Rossi, P., Buggia-Prévot, V., Clayton, B. L. L. et al. Predominant expression of Alzheimer's disease-associated BIN1 in mature oligodendrocytes and localization to white matter tracts. Molecular Neurodegeneration 11, 59 (2016). https://doi.org/10.1186/s13024-016-0124-1

36. Nott, A. et al. Brain cell type-specific enhancer-promoter interactome maps and disease-risk association. Science 366, 1134–1139 (2019). https://doi.org/10.1126/science.aay0793

37. Xiong, X., James, B. T., Boix, C. A. et al. Epigenomic dissection of Alzheimer's disease pinpoints causal variants and reveals epigenome erosion. Cell 186, 4422–4437.e21 (2023). https://doi.org/10.1016/j.cell.2023.08.040

38. Liu, Z., Zhang, S., James, B. T. et al. Single-cell multiregion epigenomic rewiring in Alzheimer's disease progression and cognitive resilience. Cell 188, 4980–5002.e29 (2025). https://doi.org/10.1016/j.cell.2025.06.031

39. de Leeuw, C. A., Mooij, J. M., Heskes, T. and Posthuma, D. MAGMA: generalized gene-set analysis of GWAS data. PLoS Computational Biology 11, e1004219 (2015). https://doi.org/10.1371/journal.pcbi.1004219

40. The 1000 Genomes Project Consortium. A global reference for human genetic variation. Nature 526, 68–74 (2015). https://doi.org/10.1038/nature15393

41. Barbeira, A. N., Dickinson, S. P., Bonazzola, R. et al. Exploring the phenotypic consequences of tissue specific gene expression variation inferred from GWAS summary statistics. Nature Communications 9, 1825 (2018). https://doi.org/10.1038/s41467-018-03621-1

42. GTEx Consortium. The GTEx Consortium atlas of genetic regulatory effects across human tissues. Science 369, 1318–1330 (2020). https://doi.org/10.1126/science.aaz1776

43. Kolberg, L. et al. g:Profiler—interoperable web service for functional enrichment analysis and gene identifier mapping (2023 update). Nucleic Acids Research 51, W207–W212 (2023). https://doi.org/10.1093/nar/gkad347

44. The Gene Ontology Consortium. The Gene Ontology knowledgebase in 2026. Nucleic Acids Research 54, D1779–D1792 (2026). https://doi.org/10.1093/nar/gkaf1292

Supplementary Files

This is a list of supplementary files associated with this preprint. Click to download.

- SupplementaryFigure1.png
- SupplementaryFigure2.png
- SupplementaryFigure4.png
- SupplementaryFigure3.png
- SupplementaryInformation.docx
- scGIPASupplementaryTablesS1S17.xlsx